Instruments and Methods

Tomography-based determination of permeability and Dupuit–Forchheimer coefficient of characteristic snow samples

Emilie ZERMATTEN,[1] Sophia HAUSSENER,[2] Martin SCHNEEBELI,[3] Aldo STEINFELD[1,4]

[1]*Department of Mechanical and Process Engineering, ETH Zürich, CH-8092 Zürich, Switzerland*
E-mail: aldo.steinfeld@ethz.ch
[2]*Department of Mechanical Engineering, Ecole Polytechnique Fédérale de Lausanne, CH-1015 Lausanne, Switzerland*
[3]*WSL Institute for Snow and Avalanche Research SLF, Flüelastrasse 11, CH-7260 Davos-Dorf, Switzerland*
[4]*Solar Technology Laboratory, Paul Scherrer Institute, CH-5232 Villigen, Switzerland*

ABSTRACT. A tomography-based methodology for the mass transport characterization of snow is presented. Five samples, characteristic for a wide range of seasonal snow, are considered. Their three-dimensional (3-D) geometrical representations are obtained by micro-computed tomography and used in direct pore-level simulations to numerically solve the governing mass and momentum conservation equations, allowing for the determination of their effective permeability and Dupuit–Forchheimer coefficient. The extension to the Dupuit–Forchheimer coefficient is useful near the snow surface, where Reynolds numbers higher than unity can appear. Simplified semi-empirical models of porous media are also examined. The methodology presented allows for the determination of snow's effective mass transport properties, which are strongly dependent on the snow microstructure and morphology. These effective properties can, in turn, readily be used in snowpack volume-averaged (continuum) models such as strongly layered samples with macroscopically anisotropic properties.

NOMENCLATURE

A_0	Specific surface (m^{-1})
c_0, c_1	Constants in Equation (2)
d	Grain diameter (m)
F_{DF}	Dupuit–Forchheimer coefficient (m^{-1})
K	Permeability (m^2)
k_4, k_5	Constants in Equation (6)
l_{REV}	Length of cubic REV
p	Pressure ($N\,m^{-2}$)
Re	Reynolds number
u_D	Darcean velocity (superficial volume-averaged velocity) ($m\,s^{-1}$)
V	Volume (m^3)
ε	Porosity
μ	Dynamic viscosity ($kg\,m^{-1}\,s^{-1}$)
Π_{pg}	Dimensionless pressure gradient
ρ	Density ($g\,m^{-3}$)
ξ	Half-bandwidth for REV determination

Subscripts

ex	Experimentally measured
num	Numerically calculated

Abbreviations

CFD	Computational fluid dynamics
CT	Computed tomography
dh	Depth hoar
DPLS	Direct pore-level simulations
ds	Decomposing snow
mI	Metamorphosed snow I
mII	Metamorphosed snow II
REV	Representative elementary volume
ws	Wet snow
RMS	Root mean square
μCT	Micro-computed tomography

INTRODUCTION

Snow, a sintered porous material made of ice grains, has a complex porous microstructure that continuously changes with time and external conditions. Its effective mass transport properties, strongly dependent on the complex microstructure, are relevant for investigating a wide range of environmental processes.

Permeability has a direct effect on snow–air exchange processes with an impact on atmosphere chemistry (Grannas and others, 2007; Clifton and others, 2008), on snow metamorphism (Albert and others, 2004) and on water flow through snow (Waldner and others, 2004). Bader (1939) gave the first quantitative data of snow permeability. Shimizu (1970) and Sommerfeld and Rocchio (1993) parameterized it in relation to density and grain size, and a permeameter for field measurements was developed by Conway and Abrahamson (1984). The experimental characterization of the effective transport properties is difficult, in part due to the rapid change of the snow's microstructure with temperature and temperature gradient (Albert and Schultz, 2002). Lately, permeability and specific surface area were used to develop a new textural characterization of snow (Arakawa and others, 2009). The Dupuit–Forchheimer coefficient is taken into account at a higher Reynolds number, when inertial effects become important (Kaviany, 1995).

Theoretical and empirical correlations for the determination of permeability have been developed for simplified

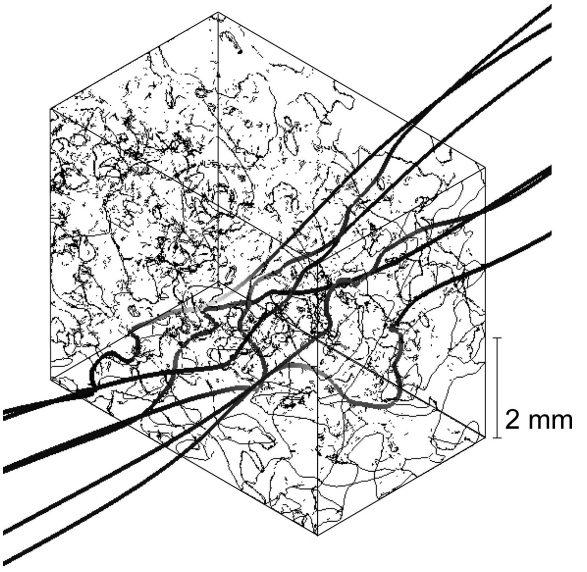

Fig. 1. 3-D surface rendering of the wet snow sample (ws, as listed in Table 1) with fluid flow streamlines.

two-phase media such as capillary drag and the Carman–Kozeny models (Ergun, 1952; Dullien, 1979; Macdonald and others, 1979; Kaviany, 1995) for fibrous beds (Davies, 1952; Chen, 1955) and cellular foams (Moreira and others, 2004). No previous studies on the Dupuit–Forchheimer coefficient of snow were found; correlations were proposed for other porous materials (Dullien, 1979; Kaviany, 1995).

Direct pore-level simulations (DPLS) have become a powerful tool for the characterization of a wide range of porous materials. In previous studies (Fredrich and others, 2006; Petrasch and others, 2008; Haussener and others, 2009, 2010), micro-computed tomography (μCT) was applied to obtain the precise digital three-dimensional (3-D) geometrical representation of complex porous media, such as reticulate ceramic foams, porous rocks and packed beds of opaque or semi-transparent particles, and subsequently used in DPLS to calculate the effective transport properties. Recently, DPLS has been applied for the characterization of polar firn (Courville and others, 2010) and shown to describe with good accuracy morphological properties as supported by experimental validation. A fundamental advantage of DPLS compared with direct measurements is that stratigraphically complex snow samples with thin layers can also be characterized, leading to different properties for each layer, whereas an experimental measurement would yield only an average over the whole sample. In the present paper, μCT is applied to obtain the 3-D digital geometry of seasonal snow types. The governing mass and momentum conservation equations are numerically solved at the pore scale (DPLS) by the finite-volume method, allowing for the determination of the permeability and Dupuit–Forchheimer coefficient.

MORPHOLOGICAL CHARACTERIZATION

Five different snow samples are considered: decomposing snow (ds), metamorphosed I (mI), metamorphosed II (mII), depth hoar (dh) and wet snow (ws). They correspond to the grain shape classifications: DFdc, RGsr/DFdc, RGsr, DHcp and MFcl (International Classification for Seasonal Snow on the Ground (ICSSG; Fierz and others, 2009)). Tomographic scans were carried out with a Scanco μCT 80 desktop X-ray tomographic set-up (Kerbrat and others, 2008). The voxel sizes were 10 μm for the ds, mI and mII snow samples, and 18 μm for the dh and ws samples, with a scanned volume of $600 \times 600 \times 400$ voxels, corresponding to 144 mm^3 and 840 mm^3, respectively. As an example, Figure 1 depicts the 3-D surface rendering of the snow sample (ws) with fluid flow streamlines.

Table 1 summarizes the morphological characteristics by experimental methods (Kerbrat and others, 2008) and by computation of the two-point correlation function and opening size distribution with spherical structuring elements on the μCT scans (Haussener, 2010). The pore and particle sizes must be read with care as they describe the smallest dimension of the pore and particle spaces, which might not characterize well the size of complex, non-spherical pores and particles.

The representative elementary volume (REV), i.e. the smallest cubic volume that can be considered as a continuum, is determined by calculating a continuum property of the sample on subsequently growing volumes until it reaches a constant value within a band of $\pm\xi$, with $\xi<1$. Figure 2 shows an example of the convergence value of the length of cubic REV calculated based on porosity for the wet snow sample with $\xi = 0.05$. The lengths of cubic REV based on porosity for the five snow samples are listed in Table 1 and are 2.4–13.8 times larger than the calculated pore and particle diameter, respectively. dh needs a relatively small REV while ws needs a relatively large REV compared with their characteristic lengths.

Table 1. Morphological characterization of snow samples. Grain shape classification (Fierz and others, 2009), measured snow density (ρ_{ex}) and voxel size (Kerbrat and others, 2008), porosity (ε_{num}), specific surface area (A_0), grain size ($d_{grain,num}$), pore size ($d_{pore,num}$) (Haussener, 2010) and edge length of cubic REV (l_{REV}) for five characteristic snow samples: decomposing snow (ds), metamorphosed I (mI), metamorphosed II (mII), depth hoar (dh) and wet snow (ws)

Sample	ICSSG	ρ_{ex}	Voxel size	ε_{num}	$A_{0,num}$	$d_{grain,num}$	$d_{pore,num}$	l_{REV}
		$g\,cm^{-3}$	μm		m^{-1}	mm	mm	mm
ds	DFdc	0.11 ± 0.01	10	0.854	8178	0.05	0.24	0.69
mI	RGsr(DFdc)	0.15 ± 0.01	10	0.845	6450	0.08	0.27	0.83
mII	RGsr	0.19 ± 0.03	10	0.805	5488	0.13	0.32	1.11
dh	DHcp	0.31 ± 0.02	18	0.670	2777	0.40	0.75	1.81
ws	MFcl	0.56 ± 0.03	18	0.384	3016	0.66	0.41	2.68

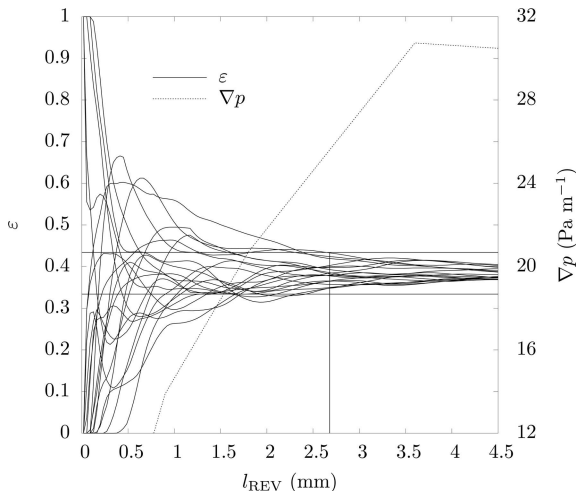

Fig. 2. Solid lines: porosity for growing cubic volumes around 20 random points for the wet snow sample. The two horizontal lines indicate the tolerance bandwidth ξ = 0.05. The vertical line indicates the chosen REV length. Dashed line: pressure drop for growing vertical length of the wet snow sample.

REV calculated based on pressure drop – and consequently on permeability and Dupuit–Forchheimer coefficient – is also shown in Figure 2, which indicates that larger REVs are required. The need for larger REV based on heat transfer properties was previously discussed (Haussener and others, 2010).

METHODOLOGY

The pressure drop over a spatially averaged isotropic porous medium is given by the extended Darcy's law (Petrasch and others, 2008; Haussener, 2010):

$$\nabla p = -\frac{\mu}{K}\overline{u}_{\mathrm{D}} - F_{\mathrm{DF}}\rho\overline{u}_{\mathrm{D}}|\overline{u}_{\mathrm{D}}|, \qquad (1)$$

where K is the permeability, F_{DF} is the Dupuit–Forchheimer coefficient, ρ is the fluid density, μ is the dynamic viscosity of the fluid and u_{D} is its superficial velocity, $|\overline{u}_{\mathrm{D}}| = \frac{1}{v}\int_v u\,\mathrm{d}V$, with volume V larger than or equal to REV. The first term is the result of viscous effects, predominant at low Reynolds numbers, whereas the second term describes the inertial effects, which become important at higher fluid velocities (Re>1) (Petrasch and others, 2008). Non-dimensionalization of Equation (1) for the one-dimensional case yields:

$$\frac{\nabla p d^2}{\mu u_{\mathrm{D}}} = \Pi_{\mathrm{pg}} = -\frac{d^2}{K} - F_{\mathrm{DF}} d\mathrm{Re} = -c_0 - c_1\mathrm{Re}, \qquad (2)$$

where d is a characteristics length scale, p is the pressure, c_0 and c_1 are constants and the normalized pressure drop Π_{pg} is linearly dependent on Reynolds number Re. The characteristic length scale, d, used throughout this study is the numerically calculated pore diameter (see Table 1). A linear least-square-fitting method was used to fit the numerically calculated Re-dependent Π_{pg}, allowing for the determination of K and F_{DF}. DPLS of fluid flow across the five characteristic snow samples was performed. An in-house tetrahedron-based mesh generator was used to create the computational grid directly on the μCT scans. A commercial CFD code (ANSYS, 2009) based on the finite volume technique was used to solve the continuity and Navier–Stokes equations.

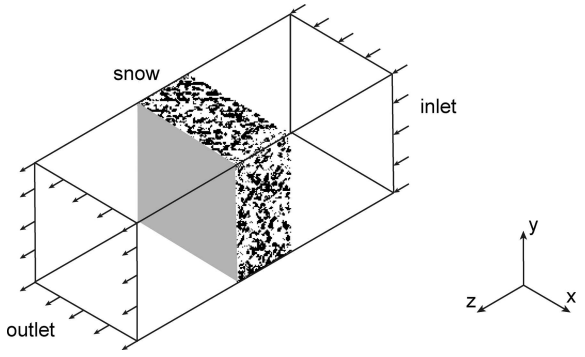

Fig. 3. Computational domain of the DPLS.

The computational domain, shown in Figure 3, consists of a square duct containing a sample of the porous material. The boundary conditions are: uniform inlet velocity and temperature and outlet pressure, no-slip and constant wall temperature at the solid–fluid interface, and symmetry at the lateral duct walls.

Preliminary calculations were carried out for various sample sizes and mesh element sizes of the subset to elucidate the trade-off between computational time and accuracy. A representative sample size of $600 \times 600 \times 200$ voxels ($10.8 \times 10.8 \times 3.6\,\mathrm{mm}^3$) with a largest mesh element size of 225 μm was chosen for ws and dh samples. For ds and mI samples, the chosen sample size was $600 \times 600 \times 300$ voxels ($6 \times 6 \times 3\,\mathrm{mm}^3$) with a largest mesh element size of 125 μm. For the mII sample, the sample size was $600 \times 600 \times 200$ voxels ($6 \times 6 \times 2\,\mathrm{mm}^3$) with a largest mesh element size of 125 μm. Convergence was achieved for a termination residual root mean square (RMS) of the iterative solution below 9×10^{-5}. The sample sizes were chosen with a relative difference in which the highest possible size was 1.7–6.2%, whereas the largest mesh element sizes were chosen with a relative difference in which the smallest possible mesh element was 2.8–10.3%. These differences were obtained by calculating the pressure drop for each mesh and sample size.

RESULTS AND DISCUSSION

The dimensionless pressure gradient Π_{pg} is plotted as a function of Re in Figure 4 for the five snow samples. The calculated permeability K and Dupuit–Forchheimer coefficients F_{DF} are plotted in Figure 5 versus the pore diameter; their values and the goodness of fit are listed in Table 2.

K is lowest and F_{DF} highest for the ws sample, as its density is highest and porosity lowest. On the other hand, K increases with ds, mI, mII and dh samples because of the

Table 2. Values of K and F_{DF} obtained by DPLS, calculated using the pore size

	ds	mI	mII	dh	ws
K (m^2)	2.73×10^{-9}	2.73×10^{-9}	3.27×10^{-9}	1.01×10^{-8}	8.49×10^{-10}
F_{DF} (m^{-1})	1.94×10^{3}	1.60×10^{3}	1.49×10^{3}	2.40×10^{3}	3.48×10^{4}
RMS	2.53	2.80	4.61	9.11	18.45

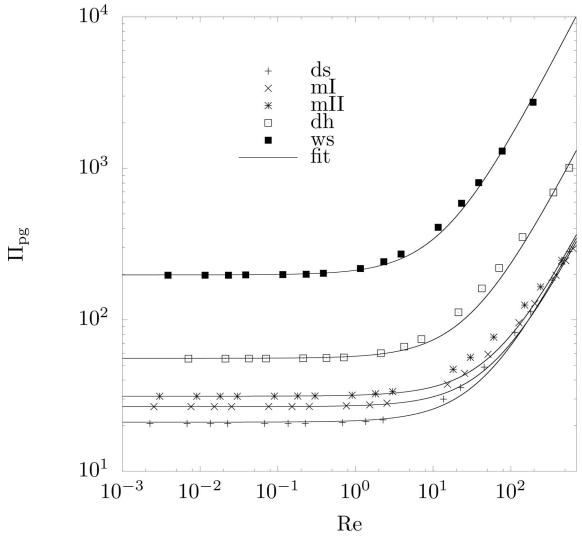

Fig. 4. Calculated (symbols) and fitted (curves) dimensionless pressure gradient as a function of Re for the five characteristic snow samples (see Table 1).

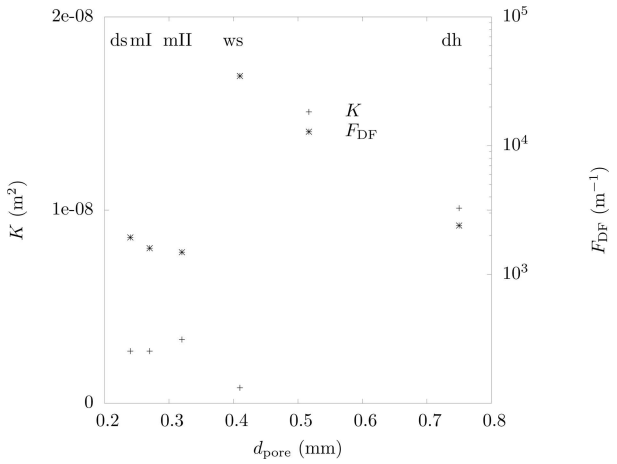

Fig. 5. Permeability and Dupuit–Forchheimer coefficient versus pore diameter.

increasing pore size, which reduces pressure loss and leads to a higher K and a smaller F_{DF} (Haussener and others, 2010). The unexpected decrease of ws in K and increase in F_{DF} highlights that one morphological characteristic (e.g. d_{pore}) does not describe sufficiently well the microstructure and supports the importance of the CT-based determination of the effective mass transport properties.

The values of K and F_{DF} of Table 2 are compared with theoretical and empirical models using simplified microstructure. The models are listed in Table 3.

The K and F_{DF} of the five characteristic snow samples, calculated by the CT-based DPLS method (Table 2) and by the simplified models of Equations (3–10), are shown in Figures 6 and 7, respectively. The conduit flow model, Equation (3), compares well with DPLS for mI, mII, dh and ds, particularly for dh (relative difference from DPLS of 17%). DPLS gives results close to those of the fibrous bed model for all types of snow (relative difference from DPLS from 18% for ws to 77% for ds). Equation (7) (Shimizu, 1970) gives values comparable to DPLS for all types of snow, but with a higher relative difference for most of them (from 41% for ds to 97% for ws). Equations (4) and (6) give results far from DPLS, with relative differences up to 4300% and 6000%, respectively. It has been shown that the Carman–Kozeny model does not fit to experimental data when the porous medium has high porosity, its particles are far from a spherical shape, or the porous medium is consolidated (Mauran and others, 2000), which is the case for snow.

Equation (8) compares well with F_{DF} values found with DPLS, in particular for mI, dh and ds, for which relative differences from DPLS are only 7%, 10% and 9%, respectively. The values obtained from Equation (9) compare well with that of DPLS, in particular for ws (relative difference of 14%). Finally, Equation (10) gives results comparable to DPLS for ws (relative difference from DPLS of 46%), but not for the other types of snow.

Table 3. Theoretical and empirical models for permeability and Dupuit–Forchheimer coefficient of porous media

Equation	Description	Equation	Source
(3)	Conduit flow model for a Hagen–Poiseuille flow	$K = \frac{\varepsilon d_{pore}^2}{32}$	Dullien (1979); Kaviany (1995)
(4)	Hydraulic radius model based on the Carman–Kozeny equation	$K = \frac{\varepsilon^3}{5(1-\varepsilon)^2 A_0^2}$	Dullien (1979); Kaviany (1995)
(5)	Empirical models for fibrous beds by Davies	$K = \frac{d_{grain}^2}{64(1-\varepsilon)^{3/2}(1+56(1-\varepsilon)^3)}$	Davies (1952); Dullien (1979)
(6)	Empirical models for fibrous beds by Chen	$K = \frac{\pi d_{grain}^2 \ln(k_5/(1-\varepsilon)^2)}{4k_4}\frac{\varepsilon}{(1-\varepsilon)}$, with $k_4 = 6.1$, $k_5 = 0.64$	Chen (1955); Dullien (1979)
(7)	Shimizu function	$K = 0.077 d_{grain}^2 \exp(-0.0078\rho)$	Shimizu (1970)
(8)	Extension of hydraulic radius theory of Carman–Kozeny	$F_{DF} = 1.8\frac{1-\varepsilon}{\varepsilon^3}\frac{1}{d_{pore}}$	Ergun (1952); Macdonald and others, (1979)
(9)	Empirical correlation for cellular foams	$F_{DF} = \frac{1.8\times10^4(1-\varepsilon)}{\varepsilon^3 d_{pore}^{0.24}}$	Moreira and others (2004)
(10)	Model relating the Dupuit–Forchheimer coefficient to the permeability	$F_{DF} = \frac{0.55}{\sqrt{K}}$	Kaviany (1995)

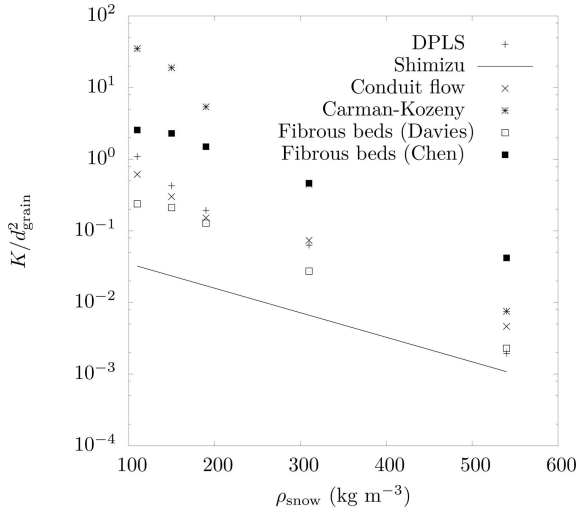

Fig. 6. Permeability (dimensionless, K/d^2_{grain}) as a function of snow density for CT-based DPLS and for theoretical and empirical models.

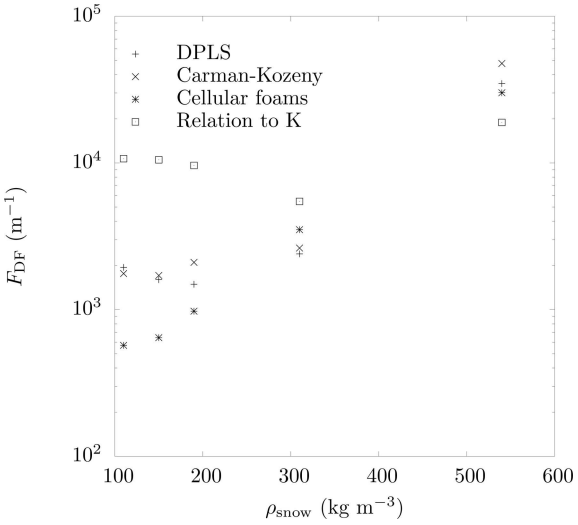

Fig. 7. Dupuit–Forchheimer coefficient as a function of snow density for CT-based DPLS and for theoretical and empirical models.

The permeability obtained by DPLS can also be compared to lattice Boltzmann modeling of permeability in firn (Courville and others, 2010). However, these results have to be taken cautiously, as the samples analyzed do not come from the same snow. Firn has generally higher grain sizes than those studied here; however, ws can be similar to small-grained firn. Permeability of ws is compared with lattice Boltzmann results in Table 4. Results are similar, however, for similar grain diameter; specific surface area is much higher in firn than in ws. This could explain the higher firn permeability. Again, this difference in specific surface area shows the high differences in microstructure.

Experimental data on the permeability of snow are scarce because handling and precise measurements are difficult. This is especially true for the more permeable snow types (e.g. depth hoar). For these snow types, DPLS will possibly become the method of choice because μCT of samples casted with diethyl phthalate has become possible (Heggli and others, 2009). Snow is often anisotropic at different scales. Even a homogeneous sample may be anisotropic in permeability at the pore level, which is accounted for in Equation (1) when introducing a permeability tensor **K** (Kaviany, 1995). The technique applied in this study is able to capture effects as previously shown for porous ceramic structures (Haussener, 2010). At a larger scale, snow is highly layered at the mm scale (Pielmeier and Schneebeli, 2003), therefore pore-level anisotropy is usually masked when measuring anisotropy in the field. DPLS is able to detect these effects and would therefore be advantageous to experimental techniques.

Table 4. Comparison of ws permeability calculated from DPLS with firn permeability obtained by lattice Boltzmann modeling (Courville and others, 2010)

	A_0	ϵ	d_{grain}	K	Difference of K with ws
	m^{-1}		mm	m^2	%
ws	3016	0.384	0.66	8.49×10^{-10}	
	7143	0.43	1.20	1.19×10^{-9}	40.2
	5882	0.43	1.31	1.67×10^{-9}	96.7
	7143	0.58	0.59	1.13×10^{-9}	33.1
	5882	0.57	0.83	2.60×10^{-9}	206.2
	6667	0.53	0.79	1.66×10^{-9}	95.5

SUMMARY AND CONCLUSIONS

Mass transfer properties, namely permeability (K) and Dupuit–Forchheimer coefficient (F_{DF}), were determined for five characteristic snow samples. The methodology involved first obtaining the complex 3-D geometrical representation of the snow microstructure by computer tomography. The μCT scans were digitalized and used in direct pore-level simulations (DPLS). An in-house tetrahedron-based mesh generator was used to create the computational grid directly on the μCT data. Mass and momentum conservation equations were numerically solved at the pore scale by the finite-volume method. Pressure drop over the snow sample was determined and fitted to Darcy's law extended by the Dupuit–Forchheimer term, allowing for the determination of K and F_{DF}. A larger pore size led to higher K, except for wet snow, for which a large pore size was compensated by a low porosity and high density.

As expected, the low K of wet snow led to a high F_{DF}. The values of K and F_{DF} computed by DPLS were compared with those obtained by analytical and empirical models of porous media with simplified microstructure. The conduit flow model compared particularly well with DPLS for four types of snow. Shimizu's prediction gave reasonable agreement. The extension of the hydraulic radius theory for F_{DF} yielded particularly good results compared with DPLS for three types of snow. The applied methodology is able to accurately account for the complex snow microstructure, which cannot be described by only a few morphological characteristics such as porosity, pore or particle size. Furthermore, it can be applied to investigate anisotropy on multiple scales. The calculated effective transport properties can be readily applied in volume-averaged (continuum) models of snowpack for a wide range of environmental applications.

REFERENCES

Albert, M.R. and E. Shultz. 2002. Snow and firn properties and air-snow transport processes at Summit, Greenland. *Atmos. Environ.,* **36**(15–16), 2789–2797.

Albert, M., C. Shuman, Z. Courville, R. Bauer, M. Fahnestock and T. Scambos. 2004. Extreme firn metamorphism: impact of decades of vapor transport on near-surface firn at a low-accumulation glazed site on the East Antarctic plateau. *Ann. Glaciol.,* **39**, 73–78.

ANSYS. 2009. *ANSYS-CFX*. Canonsburg, PA, ANSYS Inc.

Arakawa, H., K. Izumi, K. Kawashima and T. Kawamura. 2009. Study on quantitative classification of seasonal snow using specific surface area and intrinsic permeability. *Cold Reg. Sci. Technol.,* **59**(2–3), 163–168.

Bader, H. 1939. Mineralogische und strukturelle Charakterisierung des Schnees und seiner Metamorphose. *In* Bader, H. *and 6 others, eds. Der Schnee und seine Metamorphose*. Bern, Kümmerly & Frey, 1–61. (Beiträge zur Geologie der Schweiz, Geotechnische Serie Hydrologie 3.)

Chen, C.Y. 1995. Filtration of aerosols by fibrous media. *Chem. Rev.,* **55**(3), 595–623.

Clifton, A., C. Manes, J.-D. Rüedi, M. Guala and M. Lehning. 2008. On shear-driven ventilation of snow. *Bound.-Layer Meteorol.,* **126**(2), 249–261.

Conway, H. and J. Abrahamson. 1984. Air permeability as a textural indicator of snow. *J. Glaciol.,* **30**(106), 328–333.

Courville, Z., M. Hörhold, M. Hopkins and M. Albert. 2010. Lattice-Boltzmann modeling of the air permeability of polar firn. *J. Geophys. Res.,* **115**(F4), F04032. (10.1029/2009JF001549.)

Davies, C.N. 1952. The separation of airborne dust and particles *Proc. Inst. Mech. Eng.,* **1B**, 185–198.

Dullien, F.A.L. 1979. *Porous media, fluid transport and pore structure.* San Diego, CA, Academic Press.

Ergun, S. 1952. Fluid flow through packed columns. *Chem. Eng. Progr.,* **48**(2), 89–94.

Fierz, C. *and 8 others*. 2009. *The international classification for seasonal snow on the ground*. Paris, UNESCO–International Hydrological Program. (IHP Technical Documents in Hydrology 83.)

Fredrich, J.T., A.A. DiGiovanni and D.R. Noble. 2006. Predicting macroscopic transport properties using microscopic image data. *J. Geophys. Res.,* **111**(B3), B03201. (10.1029/2005JB003774.)

Grannas, A.M. *and 34 others*. 2007. An overview of snow photochemistry: evidence, mechanisms and impacts. *Atmos. Chem. Phys.,* **7**(16), 4329–4373.

Haussener, S. 2010. Tomography-based determination of effective heat and mass transport properties of complex multi-phase media. (PhD thesis, ETH Zürich.)

Haussener, S., W. Lipiński, J. Petrasch, P. Wyss and A. Steinfeld. 2009. Tomographic characterization of a semitransparent-particle packed bed and determination of its thermal radiative properties. *J. Heat Transfer,* **131**(7), 072701. (10.1115/1.3109261.)

Haussener, S., P. Coray, W. Lipiński, P. Wyss and A. Steinfeld. 2010. Tomography-based heat and mass transfer characterization of reticulate porous ceramics for high-temperature processing. *J. Heat Transfer,* **132**(2), 023305. (10.1115/1.4000226.)

Heggli, M., E. Frei and M. Schneebeli. 2009. Snow replica method for three-dimensional X-ray microtomographic imaging. *J. Glaciol.,* **55**(192), 631–639.

Kaviany, M. 1995. *Principles of heat transfer in porous media. Second edition.* New York, etc., Springer-Verlag.

Kerbrat, M., B. Pinzer, T. Huthwelker, H.W. Gäggeler, M. Ammann and M. Schneebeli. 2008. Measuring the specific surface area of snow with X-ray tomography and gas adsorption: comparison and implications for surface smoothness. *Atmos. Chem. Phys.,* **8**(5), 1261–1275.

Macdonald, I.F., M.S. El-Sayed, K. Mow and F.A.L. Dullien. 1979. Flow through porous media: the Ergun equation revisited. *Ind. Eng. Chem. Fundament.,* **18**(3), 199–208.

Mauran, S., L. Rigaud and O. Coudevylle. 2000. Application of the Carman–Kozeny correlation to a high-porosity and anisotropic consolidated medium: the compressed expanded natural graphite. *Transport in Porous Media,* **43**(2), 355–376.

Moreira, E.A., M.D.M. Innocentini and J.R. Coury. 2004. Permeability of ceramic foams to compressible and incompressible flow. *J. Eur. Ceram. Soc.,* **24**(10–11), 3209–3218.

Petrasch, J., F. Meier, H. Friess and A. Steinfeld. 2008. Tomography based determination of permeability, Dupuit–Forchheimer coefficient, and interfacial heat transfer coefficient in reticulate porous ceramics. *Int. J. Heat Fluid Flow,* **29**(1), 315–326.

Pielmeier, C. and M. Schneebeli. 2003. Developments in the stratigraphy of snow. *Surv. Geophys.,* **24**(5–6), 389–416.

Shimizu, H. 1970. Air permeability of deposited snow. *Low Temp. Sci., Ser. A,* **22**, 1–32.

Sommerfeld, R.A. and J.E. Rocchio. 1993. Permeability measurements on new and equitemperature snow. *Water Resour. Res.,* **29**(8), 2485–2490.

Waldner, P., M. Schneebeli, U. Schultze-Zimmermann and H. Flühler. 2004. Effect of snow structure on water flow and solute transport. *Hydrol. Process.,* **18**(7), 1271–1290.

MS received 1 February 2011 and accepted in revised form 14 May 2011